CHAPTER 50

On the Partition of Horizontal Momentum Between Velocity and Pressure Components Through the Transition Region of Breaking Waves

David R. Basco[1] and Takao Yamashita[2]

Abstract

When a water wave breaks, it undergoes a complicated interchange of total, depth integrated horizontal momentum between that part due to the velocity field and the part that can be assigned to the pressure distribution beneath the surface. This partition of total momentum for a strong, plunging breaker is described by a relatively crude model in which the horizontal velocity profile (over the vertical) is schematized in two layers and the pressure distribution is related to a hydrostatic distribution for the given water depth. An example calculation at four locations across the breaking transition region on a plane beach is utilized to demonstrate the principles of the model. The limitations of the approach which assumes momentum conservation in a reference frame moving with the wave celerity defined at the wave crest are presented, but await verification. The ultimate goal is a relatively simple model to predict the transition width of breaking waves (spillers, plungers and intermediate types) for plain and bar-trough beaches.

1.0 Introduction

Svendsen (1984) defined the wave breaking transition region as the distance from the break point (vertical free surface) to the transition point where the time-mean water surface changes from relatively level to an increasing slope (wave set-up). Figure 1 displays these two end points along with the plunge point (pp) and an intermediate point (ip) which shall be discussed later. At the transition point (tp), the bore-like wave with surface roller area (A) encompasses a trapped mass of fluid which is transported within the inner, surf-zone region on plane beaches.

A qualitative description of the transition region was presented by Basco (1985). The overturning, plunging jet pushes on the trough fluid ahead like a wave paddle to create the surface roller but is left behind as it generates a new, bore-like wave with completely new wave kinematics. A simple, empirically based transition zone model designed to match the Svendsen (1984) inner-region model was then presented by Basco and Yamashita (1986) at the 20th ICCE in Taiwan. The surface

---

[1]Professor of Civil Engineering and Director of Coastal Engineering Institute, Old Dominion University, Norfolk, VA 23529-0242

[2]Instructor, Disaster Prevention Research Institute, Kyoto University Kyoto 611, Japan

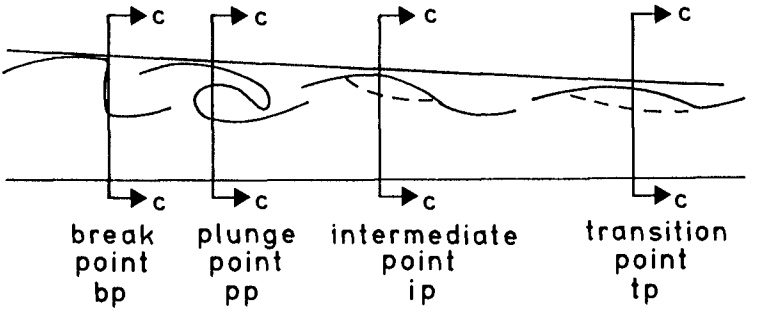

Fig. 1 Schematic of Transition and Four Key Locations

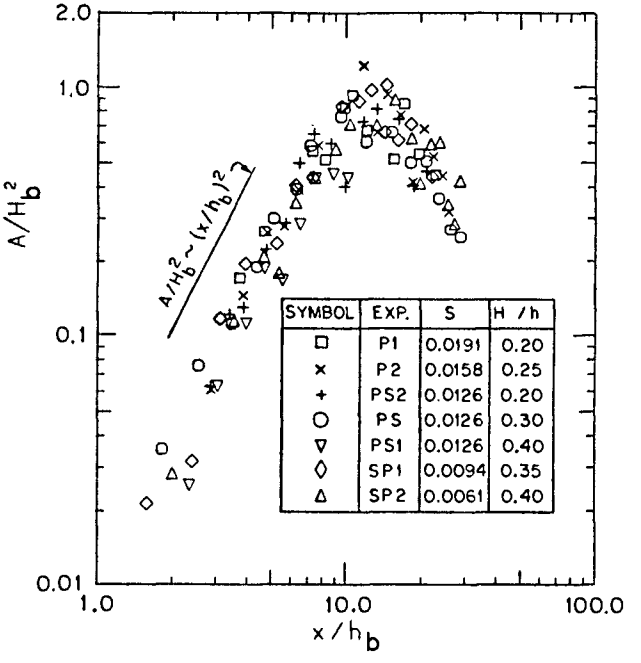

Fig. 2 Growth of Surface Roller Area With Distance From Break Point (after Papanicolaou and Raichlen, 1987)

roller area A(x) was speculated to increase linearly from zero at the plunge point to a value equal to 0.9 H^2 at the transition point as suggested by Svendsen (1984). Fig. 2 from experimental data by Papanicolaou and Raichlen (1987) suggests that A(x) varies nonlinearly as the squared distance from the plunge point to the place where A ~ 0.9 H_b^2. It is not clear however that these researchers used the same definition of surface roller area, A as first suggested by Svendsen (1984).

This paper extends these previous efforts by developing a quantitative model for the horizontal, total depth integrated momentum as partitioned between the momentum flux due to the velocity and the pressure induced momentum component. This is done in a reference frame moving with the wave celerity defined by the wave crest. Total, vertically integrated, horizontal momentum is conserved in this system.

Section 2 presents the general theory and discusses the limitations of the approach. Theoretical expressions are derived in Section 3 for the four locations in Fig. 1 and a general expression is formulated for any location. An example computation to demonstrate the plausibility of the formulations is then presented in Section 4. The paper concentrates on strong plunging breakers on a plane beach with the goal to develop relatively simple ways to predict the transition width. And, eventually to also model the transition width on a bar-trough profile where the surface roller grows and then decays rapidly as the wave "reforms" in the trough.

2.0 Theoretical Considerations

2.1 Steady Flow Momentum Balance. The vertically integrated, total horizontal momentum (m) per unit width and unit mass density (ρ) can be found from

$$m = \int_o^h \left[u^2(z) + \frac{1}{\rho} p(z) \right] dz \tag{1}$$

where z is the vertical coordinate from the floor (z = o) to the free surface (z = h) and u(z), p(z) are the horizontal velocity and pressure distributions beneath the surface, respectively. From standard definitions of the volumetric flow rate per unit width (q), momentum correction coefficient (α), and a pressure correction coefficient (a) relative to hydrostatic pressure (e.g., see Chow, 1959, p. 32) this can be written

$$m = \alpha \left[\frac{q^2}{h} \right] + a \left[\frac{1}{2} g h^2 \right] \tag{2}$$

or

$$m = m_v + m_p \tag{3}$$

so that total momentum is partitioned between the momentum flux part (m_v) and the pressure component (m_p). Four initial conditions are required to define m, namely the water depth (h), velocity magnitude (v = q/h), velocity profile (α) and pressure distribution (a).

For the classical hydraulic jump (Belanger, 1849), a uniform velocity profile ($\alpha = 1$) and hydrostatic pressure distribution ($a = 1$) are assumed both upstream and downstream of the surface roller. This reduces the problem to only two initial conditions and two unknowns so that together with the conservation of mass, a unique solution (the so-called sequent-depth equation) is possible for the downstream conditions. Madsen and Svendsen (1983) utilized a theoretical velocity profile for the flow reversal with depth through the surface roller and an empirical, vertical turbulent momentum exchange coefficient to theoretically derive the jump profile and jump length. Basco and Yamashita (1986, Fig. 6, p. 956) used this theory to present the partition of $m_v(x)$ and $m_p(x)$ across the jump. The surface roller, flow reversal causes $\alpha >> 1.0$ through the jump and results in nonlinear distributions of $m_v(x)$ and $m_p(x)$ components even though $a(x) = 1$ is taken as a first approximation.

2.2 Unsteady Flow Momentum Conservation. The integral, control volume definition of linear momentum conservation for unsteady flow can be written in vector terminology ($\vec{V}$ is the vector velocity field)

$$\int_V \frac{\partial(\rho\vec{V})}{\partial t}\, dV + \int_s (\rho V)\, \vec{V} \cdot d\vec{s} = \Sigma \vec{F} \qquad (4)$$

the first term (LHS) is the unsteady flow contribution over the control volume (V) and the second is the momentum flux through the control surface (s). The RHS is the sum of all external forces (F) responsible for the changes taking place on the LHS.

In this paper, we make the unproven assumption that the unsteady, time-derivative term on the LHS is small relative to the other terms in the momentum balance. Therefore we neglect the time-derivative term in this paper. For a breaking/broken water wave with dominant flow direction parallel to the bottom, the momentum balance in this direction is then given by Eqn (1) if we also neglect the boundary shear stress. And, if we operate in a moving coordinate system.

2.3 Non-accelerating Coordinate System. We can perform a Galilean transformation of our momentum conservation equation by moving our control volume at constant speed, i.e., by using a non-accelerating coordinate system. To remain phase locked with the wave crest we can use the wave propagation celerity as defined by the crest.

In this paper, we make the experimentally demonstrated assumption that the breaking/broken wave celerity through the transition region is approximately constant (see e.g., Basco, 1985, Fig. 4, p. 175).

2.4 Time-averaged Momentum Balance. Time-averaging Eqn (1) and then subtracting the hydrostatic pressure force measured from the mean water surface ($\bar{\eta}$) for a water wave produces the wave-induced momentum thrust or radiation stress. Across the transition region, by definition, $\bar{\eta}$ is constant so that if we again neglect the bottom shear stress, the radiation stress must also be constant based on the time-averaged momentum balance. One way for this to occur is for each phase-locked section of the breaking/broken wave moving through the transition to have constant total momentum. This gives added confidence to our assumptions cited above.

3.0 Transition Region Theory

3.1 Definitions. Consider the velocity profile u(z) beneath a breaking wave as shown in Fig. 3 relative to a fixed reference frame. We schematize the velocity distribution into two major segments; (1) a crest region velocity $V_c(x)$ and (2) a trough region velocity $V_t(x)$ that act over b(x) and d(x), respectively. Note that one key feature of wave breaking is that the crest region and trough region absolute* velocities are in opposite directions.

It is useful to define the following dimensionless ratios using the wave crest celerity (c) as the reference velocity:

$$\lambda \equiv \frac{V_c}{c} \tag{5}$$

$$\xi \equiv \frac{|V_t|}{V_c} \tag{6}$$

therefore

$$\lambda\xi = \frac{|V_t|}{c} \tag{7}$$

The wave crest celerity for shallow water wave breaking is approximately

$$c^2 \simeq gh_c \tag{8}$$

where h_c is the total water depth at the wave crest.

3.2 Moving Reference Momentum Balance. The counterpart of Eqn (1) for a control volume moving with speed (c) is

$$m^* \equiv \int_o^h \left\{ [u(z) + c]^2 + \frac{1}{\rho} p(z) \right\} dz \tag{9}$$

or

$$m^* = m_v^* + m_p^* \tag{10}$$

where now total relative momentum (m*) is partitioned into relative velocity (m_v^*) and pressure (m_p^*) components.

3.3 Schematized Transition - Strong Plunging Breaker. Using the qualitative model and ideas presented in Basco (1985), we schematically depict the velocity and pressure distributions for a strong, plunging breaker on a plane beach in Fig. 4. The crest velocity begins to exceed the wave celerity ($\lambda \geq 1$) at the break point and continuity results in $\lambda \gg 1$ at the plunge point for a strong plunging jet. At this point, the surface roller begins to form ($A \geq 0$) and grows in size as the plunging jet slows down ($\lambda < 1$) and exchanges its momentum through turbulent shear stresses with the trough fluid below. The overturning jet of a

*Absolute when referenced to a fixed (Eulerian) observer.

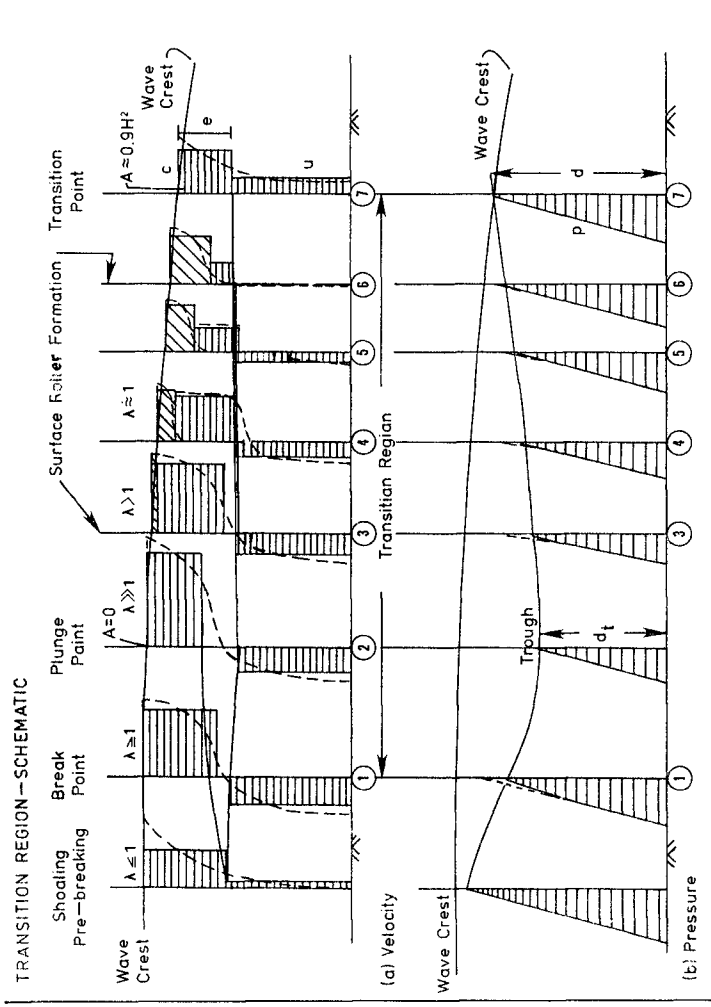

Fig. 4 Schematized Velocity and Pressure Distributions Across Transition Region (following qualitative model of Basco, 1985)

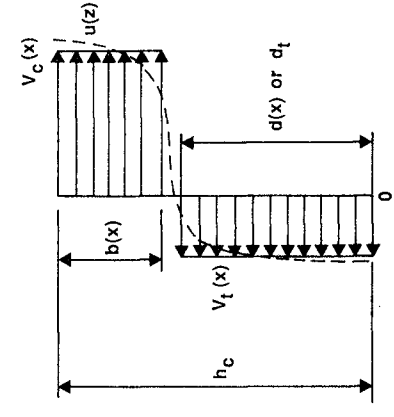

Fig. 3 Schematized Horizontal Velocity Distribution Beneath Crest Region of Breaking Wave

breaking wave can be seen to perform two primary tasks in the transition region, namely:

(1) to create a surface roller, with trapped mass of fluid that propagates with the wave celerity, and

(2) to reverse the direction of the trough velocity from that opposing the crest, to that in the same direction as the particles in the surface roller.

At the transition point, or end of the transition region, the velocity profile beneath the crest is that of a propagating bore (Svendsen, 1984).

The corresponding pressure distribution changes are also shown in Fig. 4. Streamline curvature causes the pressure to remain less than hydrostatic ($a < 1$) through the break point. The pressure within the plunging jet is essentially zero if we assume it behaves as a free jet so that the pressure falls to essentially that approximated by hydrostatic pressure in the trough fluid. The pressure distribution then rises again to reach full hydrostatic pressure ($a = 1$) at the transition point.

These schematic ideas are translated into quantifiable relations at four representative locations within the transition region.

(i) Break Point (bp)

Fig. 5 depicts the absolute velocity structure ($\xi < 1$) and assuming $\lambda \doteq 1$ ($V_c \doteq c$), the velocity distribution for an observer moving with the wave crest, i.e., the relative velocity is also shown acting over the depths indicated. The velocity momentum (m_V^*) is then given by

$$m_V^* = (V_t + c)^2 d_t = [(\lambda\xi)c + c]^2 d_t = c^2(\lambda\xi + 1)^2 d_t \qquad (11)$$

and is taken here to act over the depth (d_t) which is essentially the trough depth for a strong plunging breaker. Using Eqn (8) for c^2 and multiplying by unity (h_c/h_c) gives

$$m_V^* = \left[\frac{d_t}{h_c}\right](\lambda\xi + 1)^2 \, gh_c^2 \qquad (12)$$

The first two terms in parentheses are dimensionless so that the last term (gh_c^2) gives the physical scale to the momentum and/or can be used to normalize the equation.

The pressure related momentum is simply

$$m_p^* = (a)\left[\frac{1}{2}gh_c^2\right] \qquad (13)$$

so that the total, relative momentum at the break point (m_{bp}^*) becomes

$$m_{bp}^* = \left[\left[\frac{d_t}{h_c}\right](\lambda\xi + 1)^2 + \frac{1}{2}\,a\right] gh_c^2 \qquad (14)$$

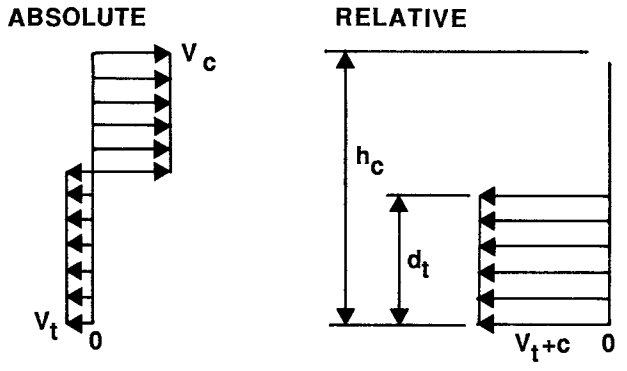

Fig. 5 Break Point - Absolute and Relative Velocities

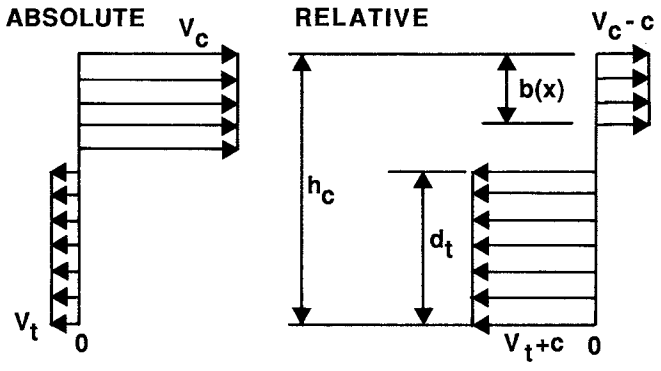

Fig. 6 Plunge Point - Absolute and Relative Velocities

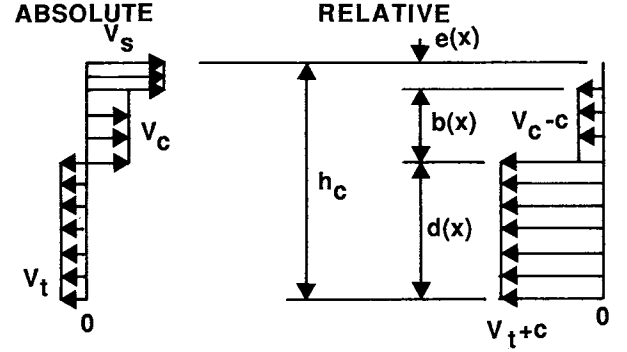

Fig. 7 Intermediate Point-Absolute and Relative Velocit.

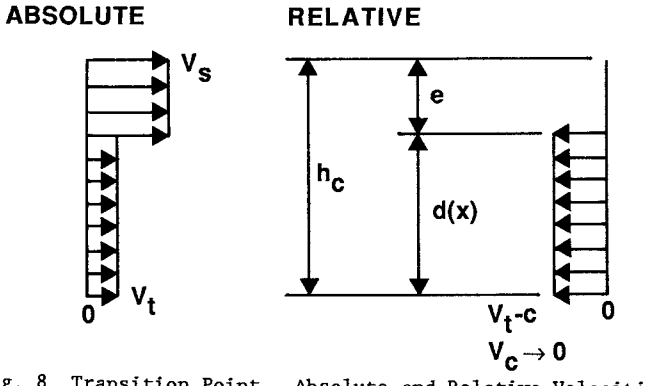

Fig. 8 Transition Point - Absolute and Relative Velocities

Four quantities must be specified [(d_t/h_c), ξ, a, and h_c] to define m^*_{bp} if we assume $\lambda = 1$ at the break point.

Using the trough relative Froude number (F^*_t) as a measure of the strength of the breaking wave defined as (Stive, 1984)

$$(F^*_t)^2 \equiv \frac{(V_t + c)^2}{gd_t} \tag{15}$$

this becomes at the break point

$$(F^*_t)^2 = (\lambda\xi + 1)\left[\frac{h_c}{d_t}\right]^{1/2} \tag{16}$$

or combining Eqn (12) and (16) we have

$$(F^*_t)^2 = \frac{m^*_v}{gh_c^2}\left[\frac{h_c}{d_t}\right]^2 \tag{17}$$

so that we need only two quantities (d_t/h_c and ξ) to specify the incoming relative Froude number if we again take $\lambda = 1$ at the wave breaking point.

(ii) Plunge Point (pp)

Now, $\lambda > 1$ ($V_c > c$) and again taking $\xi < 1$ as depicted in Fig. 6 with V_c acting over a contracted, free jet width b(x) with p = o gives

$$m^*_v = \left[\frac{d_t}{h_c}(\lambda\xi + 1)^2 + \frac{b(x)}{h_c}(\lambda - 1)^2\right] gh_c^2 \tag{18}$$

with the plunging jet now contributing to the relative momentum as given by the second term within the brackets.

With the pressure zero in the overturning jet, the pressure momentum coefficient a becomes

$$a = \frac{1/2gd_t^2}{1/2gh_c^2} = \left[\frac{d_t}{h_c}\right]^2 \tag{19}$$

if we assume the streamlines within the trough are relatively flat to create a hydrostatic pressure distribution. This then results in

$$m^*_p = \left[\frac{1}{2}\left[\frac{d_t}{h_c}\right]^2\right] gh_c^2 \tag{20}$$

when the wave crest height h_c is used as reference. Combining gives for total relative momentum at the plunge point (m^*_{pp})

$$m^*_{pp} = \left[\left[\frac{d_t}{h_c}\right](\lambda\xi + 1)^2 + \frac{b(x)}{h_c}(\lambda - 1)^2 + \frac{1}{2}\left[\frac{d_t}{h_c}\right]^2\right] gh_c^2 \tag{21}$$

Comparing Eqn (14) at the break point and (21) we see that if total, relative momentum is conserved, and when the first term within the brackets also remains relatively unchanged, then the added momentum of the overturning jet is balanced by the decreased pressure momentum within the trough. Four quantities [d_t/h_c, b/h_c, λ, and h_c] must again be specified to calculate m^*_{pp} if we now also assume that ξ remains the same as at the break point.

(iii) Transition Point (tp)

Now lets move to the end of the transition region and consider the transition point (t_p) as depicted in Fig. 8. We here define the velocity in the trapped surface roller as V_s to distinguish it from that within the plunging jet (V_c) that is slowing down and being left behind [$\lambda \to o$, $b \to o$]. The surface roller area (A) grows as shown in Fig. 2 and consequently so does the thickness of the trapped surface roller (e).

The relative velocity momentum becomes

$$m^*_v = \left[\frac{d(x)}{h_c}(\lambda\xi - 1)^2\right] g h_c^2 \tag{22}$$

and the fact that the trough velocity V_t is now in the same direction as the wave celerity produces the negative sign within the bracketed term. This translates into a decrease in relative importance in the velocity component of the total momentum.

The pressure component must therefore increase and we take a = 1 to give full hydrostatic pressure as a first approximation, or

$$m^*_p = \frac{1}{2} g h_c^2 \tag{23}$$

so that the total relative momentum at the transition point (m^*_{tp}) becomes

$$m^*_{tp} = \left[\frac{d}{h_c}(\lambda\xi - 1)^2 + \frac{1}{2}\right] g h_c^2 \tag{24}$$

We again need four quantities [d/h_c (or e/h_c), λ, ξ and h_c] to compute m^*_{tp}.

(iv) Intermediate Point (ip)

This is obviously the most complicated region between the plunge and transition points (see Fig. 4). The plunging jet velocity slows down ($V_c < c$) as the surface roller moving with the phase speed ($V_s = c$) expands from e = o at the plunge point to e at the transition point where $A = 0.9\ H_b^2$. The most important physical factor is the reversal in direction of V_t so that the ($\lambda\xi + 1$) term becomes ($\lambda\xi - 1$). Also V_t acts over an expanding width d(x) as $b(x) \to o$ which is a consequence of the turbulent mixing between the jet and trough fluids. Fig. 7 depicts both absolute and relative velocity distributions at an intermediate point where the trough velocity is still opposing the wave celerity. In general, the velocity momentum can be written

$$m_v^* = \left[\frac{d(x)}{h_c}(\lambda\xi \pm 1)^2 + \frac{b(x)}{h_c}(\lambda - 1)^2\right] g h_c^2 \qquad (25)$$

and the pressure momentum

$$m_p^* = \left[\frac{1}{2}a\right] g h_c^2 \qquad (26)$$

so that the total relative momentum at an intermediate position becomes

$$m_{ip}^* = \left[\frac{d(x)}{h_c}(\lambda\xi \pm 1)^2 + \frac{b(x)}{h_c}(\lambda - 1)^2 + \frac{1}{2}a\right] g h_c^2 \qquad (27)$$

Eqn (27) reduces Eqn (14) at the break point, to Eqn (21) at the plunge point and to Eqn (24) at the transition point when the appropriate assumptions are made. Consequently it is also the general expression for total relative momentum anywhere within the transition region.

In general, six quantities [d/h_c, λ, ξ, b/h_c, a, h_c] are needed to use Eqn (27). Two additional expressions can be e(x) as related to A(x) and some relation for $b(x) \to o$ in the overturning jet along with the fact that $e(x) + b(x) + d(x) = h_c$.

4.0 An Example Computation

Consider a strong plunging breaker on a plane beach with crest height h_c of 13.5 ft (4.1m) at the instant of breaking. The water depth in the trough, immediately ahead is about one-half this depth (d_t/h_c = 0.5) and the trough velocity is about 20% of the crest velocity (ξ = 0.2, Stive, 1984). The situation is schematized in Fig. 9 and summarized in Table I. Assume also that at the instant of breaking (front wave face is vertical) the streamline curvature is such that the pressure coefficient a is 0.6. Using Eqn. (14), the relative velocity momentum, m_v^* is calculated to be 4221 ft^3/sec^2 (120 m^3/s^2) and the pressure momentum, m_p^* is 1759 ft^3/sec^2 (49 m^3/s^2) resulting in a total relative momentum, m^* of 5980 ft^3/sec^2 (169 m^3/sec^2). In other words, the total momentum is about 6000 ft^3/sec^2 of which the initial partition at breaking results in 71 percent due to velocity and 29 percent due to pressure.

From Eqn (16), the relative trough Froude number, F_t^* is 1.7. This value would indicate a strong plunging breaker (spilling breakers have much lower values) but a weak bore or hydraulic jump. The fluid flow in the trough in the relative, moving coordinate system is supercritical.

As the wave overturns, the crest height (h_c) decreases. The example shows h_c values (col 3) of 13.1 ft (4.0m) at the plunge point, 12.7 ft (3.9 m) at the intermediate point, and 12.3 ft (3.7m) at the transition point or end of the transition region. These values were estimated for this example although they also could have been calculated if the total relative momentum m* was assumed constant at 6000 ft^3/sec^2.

The example shows that using these h_c values and the other given conditions which are all plausible and or referenced magnitudes, that

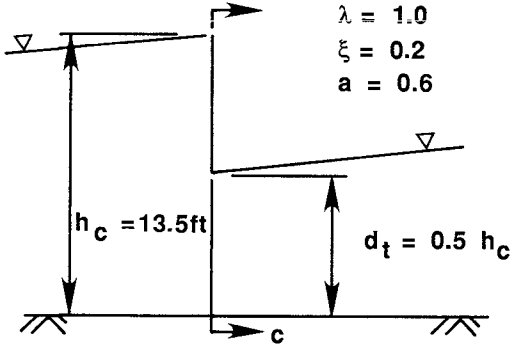

Fig. 9 Break Point - Given Conditions

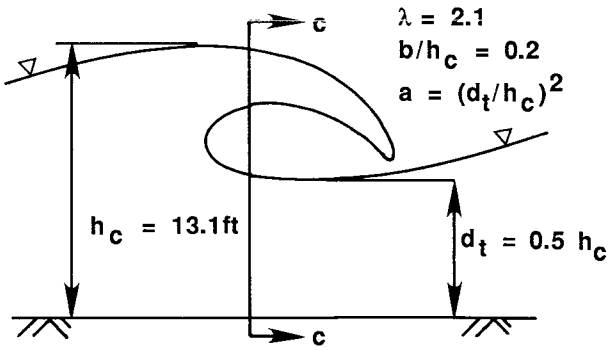

Fig. 10 Plunge Point - Given Conditions

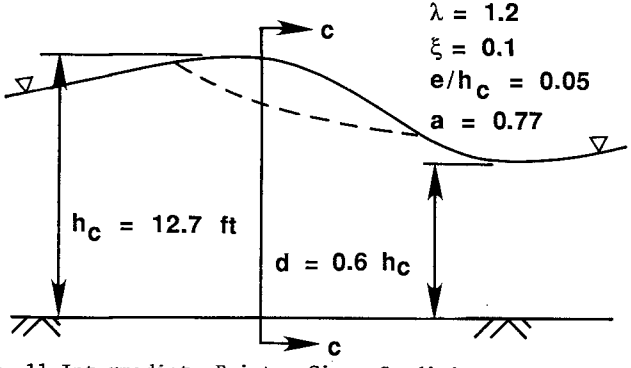

Fig. 11 Intermediate Point - Given Conditions

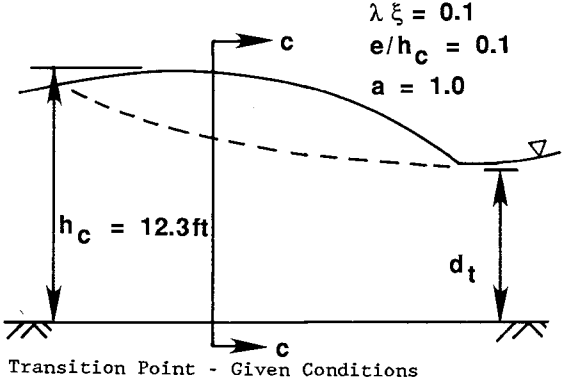

Fig. 12 Transition Point - Given Conditions

Table I - An Example Computation for Strong, Plunging Breaker on Plane Beach

Location (Equation)	Fig. Nos.	Given Conditions [reference]						m_v^* ft^3/sec^2			m_p^*	m*	
		h_c ft (m)	$\frac{d}{h_c}$			$\frac{b}{h_c}$ or $\frac{e}{h_c}$	a	$\frac{d}{h_c}(\lambda\xi\pm1)$ (m^3/s^2)	$\frac{b}{h_c}(\lambda-1)^2$ (percent of m*)	Total m_v^* (percent of m*)	$\frac{1}{2}agh_c^2$ (percent of m*)	Total Relative Momentum (m^3/s^2)	Remarks
(1)	(2)	(3)	(4)	(5)	(6)	(7)	(8)	(9)	(10)	(11)	(12)	(13)	(14)
Break Point Eqn (14)	5,9	13.5 (4.1)	0.5 (trough)	1.0 (assume)	0.2 [9]	-	0.6	4221 (120)	0	4221 (71%)	1759 (29%)	5980 (169)	Velocity Dominates
Plunge Point Eqn (21)	6,10	13.1 (4.0)	0.5 (trough)	2.1 [5,6]	$\lambda\xi$ same as b_p	0.2 [5]	$\frac{d_t^2}{h_c}$	3975 (113)	1325 (22%)	5300 (88.5%)	690 (11.5%)	5990 (170)	Velocity Nearly 90% of Total
Inter. Point Eqn (27)	7,11	12.7 (3.9)	0.6	1.2	0.1	(0.05)	0.77	3905 (111)	73 (2%)	3978 (66.6%)	1998 (33.4%)	5976 (169)	
Transition Point Eqn (24)	8,12	12.3 (3.7)	-	$\lambda\xi = 0.1$ [9]		0.1 [10]	1.0 (assume)	3553 (101)	0	3553 (59%)	2433 (41%)	5986 (169)	Velocity Still Dominates But to Less Extent

the partition of momentum changes through the transition. At the plunge point, we have taken the value of $\lambda\xi$ the same as at the break point but increased λ to over 2 as demonstrated numerically by Cokelet (1976) and experimentally by Kjeldsen (1984). The result is more velocity momentum with m_v^* now being 5300 ft^3/sec^2 (150 m^3/s^2) or almost 89 percent of the total. And, a full 22 percent of the total is found in the jet momentum. The pressure component drops to only 960 ft^3/sec^2 (20 m^3/sec^2) which is 11 percent of the total m* of 5990 ft^3/sec^2 (170 m^3/s^2).

At the intermediate section, the pressure begins to recover with m_p^* now 1998 ft^3/sec^2 (57 m^3/s^2) or 33.4 percent. The velocity momentum, m_v^* has dropped to 3978 ft^3/sec^2 (113 m^3/s^2) or 66.6 percent and of this amount, only 73 ft $^3/sec^2$ (2 m^3/sec^2) remains in the crest region due to the plunging jet. Clearly, the original, plunging jet momentum is decaying and being left behind.

At the end of the transition region, the pressure component (m_p^*) has now risen to 2433 ft^3/sec (69 m^3/s^2) or 41% of the total which is the highest across the entire region. Conversely, the relative velocity momentum, m_v^* is the lowest [3553 ft^3/sec^2, (101 m^3/s^2), 59 percent] since all the particles beneath the crest are now traveling in the same direction as the wave. The given conditions employed in these calculations were aided by experimental data found in Stive (1988) and Svendsen (1984). At the end of the transition region, the relative velocity momentum still dominates the pressure component but to a far lesser extent.

5.0 Summary

All of these values are summarized in Fig. 13 for the four "points" across the transition region. Smooth curves have been drawn in to demonstrate the momentum partition trends for this example. These results, although a delicate balance and sensitive to the individual values used for each given condition at each section, can be looked upon as somewhat indicative of the general trends that must be present, namely:

(i) the velocity dominates in all cases and is largest at the plunge point of a strong, plunging breaker;

(ii) the trough velocity is the key variable, and the physical processes present to reverse its direction dominate the transition region; and

(iii) the pressure is secondary in all cases and is smallest at the plunge point, then recovers to attain its greatest influence at the end of the transition region.

For a strong, plunging breaker on a plane beach and within the limitations and assumptions made throughout, we have developed a crude, quantitative model of the relative momentum and its partition. The role of the plunging jet momentum is to (1) form a surface roller and (2) reverse the trough flow direction over the trough depth. It becomes quite apparent that the relative strengths of the plunging jet momentum and the trough momentum control the time and hence spacial extent over which this transition process takes place. At one extreme is a relatively rapid, short transition as in this example for the strong

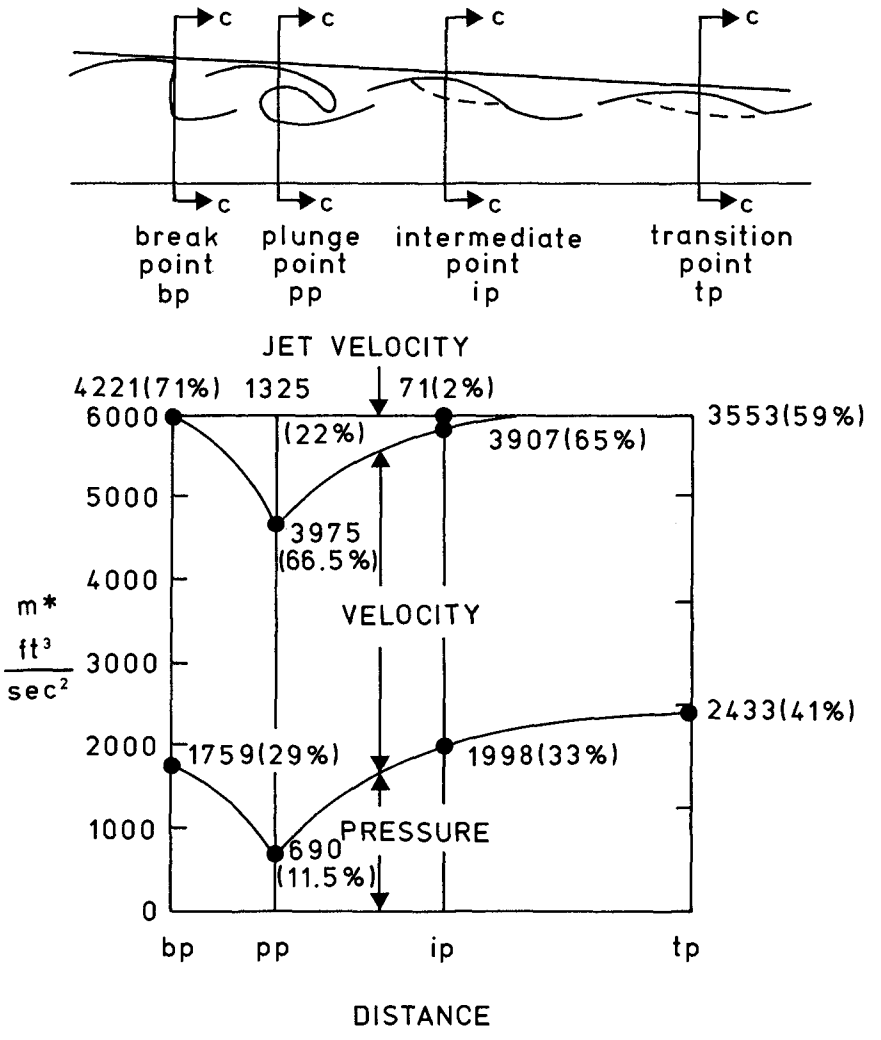

Fig. 13 Summary of Example Computation Across Transition Region

plunger.

The opposite extreme is a weak spilling breaker. The small overturning jet at the crest is still present but barely discernable. It's role remains the same but the transition requires a wide distance for the full surface roller to form and for the trough flow to be reversed over the entire vertical depth.

However, in both extremes, the strength of the trough velocity is believed to be the key variable. In nature, at some beaches, we can simultaneously observe waves breaking on relatively plane sections, waves breaking on bars and reforming in the deeper trough regions and waves breaking in the swash zone right on the beach. In all cases, the strength of the return flow in the trough appears to control the entire process. Consequently, it is felt that future numerical and experimental research (both laboratory and field) on breaking waves should give greater emphasis to defining the character of the trough flow.

References

1. Basco, D.R., (1985) "A Qualitative Description of Wave Breaking", Journ WW, ASCE, Vol. III, No. 2, Mar., pp. 171-188.

2. Basco, D.R. and T. Yamashita (1986), "Toward A Simple Model of the Wave Breaking Transition Region in Surf Zones", Proceedings, 20th ICCE, Taiwan, Vol. II, pp. 955-970.

3. Chow, V.T. (1959), Open-Channel Hydraulics, McGraw-Hill, N.Y.

4. Cokelet, E.O. (1978), "The Plunging Jet of a Breaking Wave", Euromech 102 (Breaking Waves: Surf and Run-Up on Beaches), Univ. of Bristol, England, July

5. Kjeldsen, S.P. (1984), "The Experimental Verification of Numerical Models of Plunging Breakers", 19th ICCE Proceedings, Vol. I, pp. 15-30.

6. Madsen, P.A. and I.A. Svendsen (1983), "Turbulent Bores and Hydraulic Jumps", Journal Fluid Mechanics, Vol. 129, pp. 1-25.

7. Papanicolaou, P. and F. Raichlen (1987), "Wave Characteristic in the Surf Zone", Proceedings Coastal Hydrodynamics 87, ASCE, NY, p. 765-780.

8. Stive, M.J.F. (1980), "Velocity and Pressure Field of Spilling Breakers", Proceedings, ICCE, 17th, pp. 547-566.

9. Svendsen, I.A. (1984), "Wave Heights and Set-Up in a Surf Zone", Coastal Engineering, Vol. 8, pp. 303-329.